

Electronic Supplementary Information (ESI) for

**Mechanochemical Synthesis of 0D and 3D Cesium Lead Mixed Halide
Perovskites**

Abhoy Karmakar, Mya S. Dodd, Xiaoyue Zhang, Meagan S. Oakley, Mariusz Klobukowski and
Vladimir K. Michaelis*

Department of Chemistry, University of Alberta, Edmonton, Alberta, T6G 2G2, Canada

**Corresponding author: vladimir.michaelis@ualberta.ca*

Table of Contents

<u>Content</u>	<u>Page #</u>
Materials and Methods	S1-S6
Table S1. ^{207}Pb and ^{133}Cs NMR parameters for 3D CsPbX_3 ($X = \text{Cl, Br, I}$) and 0D Cs_4PbX_6 ($X = \text{Cl, Br}$) parent perovskites ($B_0 = 11.75$ T).	S6
Table S2. ^{207}Pb magnetic shielding parameters from octahedral $[\text{PbX}_{6-x}\text{X}'_x]^{4-}$ anionic clusters from DFT calculations.	S7
Figure S1. Room temperature powder XRD patterns for $\text{CsPbCl}_x\text{Br}_{3-x}$ (a), and $\text{CsPbBr}_x\text{I}_{3-x}$ (b), where $0 \leq x \leq 3$.	S8
Figure S2. Photos of the 3D materials (a). Normalized absorbance spectra and direct bandgap relationship with halide composition for $\text{CsPbCl}_x\text{Br}_{3-x}$ (b and d, respectively) and $\text{CsPbBr}_x\text{I}_{3-x}$ (c and e, respectively), where $0 \leq x \leq 3$.	S8
Figure S3. Room temperature ^{207}Pb NMR spectra acquired at 11.75 T under non-spinning conditions for $\text{CsPbCl}_x\text{Br}_{3-x}$ (a), and $\text{CsPbBr}_x\text{I}_{3-x}$ (b), where $0 \leq x \leq 3$.	S9
Figure S4. ^{207}Pb (a) and ^{133}Cs (b) NMR spectra for $\gamma\text{-CsPbI}_3$ (perovskite or black phase) and for $\delta\text{-CsPbI}_3$ (non-perovskite or yellow phase), acquired at 11.75 T.	S9
Figure S5. ^{207}Pb NMR spectra for $\text{CsPbCl}_{1.5}\text{Br}_{1.5}$ MHP (a, 3D material) and $\text{Cs}_4\text{PbCl}_3\text{Br}_3$ MHP (b, 0D material) prepared by MCS, acquired at 11.75 and 21.1 T under non-spinning sample conditions.	S10
Figure S6. Room temperature ^{133}Cs NMR spectra acquired at 11.75 T with an MAS frequency of 13 kHz for the $\text{CsPbCl}_x\text{Br}_{3-x}$ (a), and $\text{CsPbBr}_x\text{I}_{3-x}$ (b) series, where $0 \leq x \leq 3$. The linear fitting of ^{133}Cs isotropic chemical shifts vs bromine mole-fraction for the $\text{CsPbCl}_x\text{Br}_{3-x}$ series is shown in (c).	S11
Figure S7. Room temperature XRD and ^{133}Cs NMR of comparison of 0D Cs_4PbX_6 , 2D CsPb_2X_5 , 3D CsPbX_3 and CsX ($X = \text{Cl, Br}$).	S12
Figure S8. Room temperature ^{133}Cs NMR spectra for CsPbI_3 (a) showing the perovskite, $\gamma\text{-CsPbI}_3$, to non-perovskite, $\delta\text{-CsPbI}_3$, phase conversion over time.	S13
Figure S9. Room temperature non-spinning ^{207}Pb - ^{207}Pb EXSY NMR spectra for 3D $\text{CsPbCl}_{1.5}\text{Br}_{1.5}$ and 0D $\text{Cs}_4\text{PbCl}_3\text{Br}_3$ MHP materials acquired at 21.14 T with a mixing time of 20 ms.	S13
Figure S10. Calculated ^{207}Pb NMR isotropic chemical shift with Br substitution in $[\text{PbCl}_{6-x}\text{Br}_x]^{4-}$ polyhedral (a, 3D materials), I substitution in $[\text{PbBr}_{6-x}\text{I}_x]^{4-}$ polyhedral (b, 3D materials), and Br substitution in $[\text{PbCl}_{6-x}\text{Br}_x]^{4-}$ polyhedral (c, 0D materials), where, $x = 0$ to 6.	S14
References	S15

Experimental

Materials and Methods

All starting precursor materials were obtained from commercial sources and used without further purification: lead (II) iodide (99%), lead (II) bromide (+98%) and lead (II) chloride (99%) from ACROS Organics (Morris Plains, NJ, USA); CsBr, CsCl, and CsBr from Sigma Aldrich.

Mechanochemical Synthesis of 3D CsPbX₃X'_{3-x} (X and X' = Cl, Br, I and x = 0 to 3):

Mechanochemical synthesis (MCS) has become a popular solvent-free method to obtain inorganic and organic-inorganic metal halide perovskite materials.¹⁻⁸ Using a similar approach 3D LHP parent compounds and their respective MHPs were prepared by the MCS route via manual hand grinding (HG) using a mortar and pestle for 2 hours under ambient conditions. To achieve the desired composition of the final product, the appropriate molar ratio of the starting material was loaded. For example, to synthesize (i) the parent compounds, CsPbX₃ (X = Cl, Br and I), 1:1 molar ratios of CsX and PbX₂ were used as the starting materials, (ii) MHPs like CsPbCl_{1.5}Br_{1.5}, equimolar amounts of CsCl, CsBr, PbCl₂ and PbBr₂ were used. The phase purity of the MCS products were examined using powder XRD after the synthesis. For CsPbX₃ (X = Cl and Br) and Cl/Br MHPs (CsPbCl₃Br_{3-x}), desired perovskite phases were obtained by the MCS-HG process (confirmed by powder X-ray diffraction (XRD)). For CsPbI₃ and Br/I MHPs (CsPbBr₃I_{3-x}), yellowish coloured non-perovskite phases were obtained by MCS-HG and thus they were further treated by thermal annealing (220-350 °C) under ambient conditions.

Mechanochemical Synthesis of 0D Cs₄PbX₆X'_{6-x} (X and X' = Cl, Br and x = 0 to 6):

Zero dimensional Cs₄PbX₆ (X = Cl, Br) parent and Cs₄PbCl₃Br₃ MHP compounds were prepared by the MCS route via manual hand grinding using a mortar and pestle for 2 hours under ambient conditions. To achieve the desired composition of the final product, the appropriate molar ratio of the starting material was loaded. For example, to synthesize (i) the parent compounds, Cs₄PbX₆ (X = Cl, Br), 4:1 molar ratios of CsX and PbX₂ were used as the starting materials, (ii) Cs₄PbCl₃Br₃ MHP, CsCl, CsBr,

PbCl₂ and PbBr₂ were used with a molar ratio of 4:4:1:1. The phase purity of the MCS products were examined using XRD after the synthesis. Unfortunately, obtaining a phase-pure Cs₄PbI₆ material using the same approach was unsuccessful.

Worth noting are two minor impurity phases that appear during the MCS of 0D LHPs. We can clearly identify one as the starting material (CsX, *ca.* 1%), while the other is an unidentified Cs-containing phase (*ca.* 5%) as shown in Fig. 1f and S7. We further note these two impurities remain unaltered upon further hand grinding (i.e. up to 1 hour). MCS is a suitable synthesis approach to avoid other stable ternary cesium lead halide compounds such as 3D CsPbX₃ and 2D CsPb₂X₅ impurities as indicated by ¹³³Cs NMR analysis (Fig S7).

Powder X-ray Diffraction (XRD):

The XRD measurements were obtained under ambient laboratory conditions on an Inel MPD multi-purpose diffractometer (40 kV, 50 mA) system (Department of Chemistry, University of Alberta) equipped with a CPS 120 curved position sensitive X-ray detector and Cu K_α radiation source (1.540596 Å). All the samples were placed on a plastic sample holder and 2θ scans between 0° to 114° with a step increment of 0.029° were obtained.

Diffuse Reflectance (DR) Spectroscopy:

The DR spectra of the samples were collected on a Cary 5000 UV/Vis/NIR spectrophotometer (Analytical and Instrumental Laboratory, Department of Chemistry, University of Alberta), equipped for the analysis of small-quantity fine powdered samples. Each sample (~ 50 to 100 mg) was packed into a black boat and measurement was acquired between 200 and 1000 nm wavelength with a 100 % reflectance standard.

The DR spectra were converted to pseudo-absorbance spectra using the following Kubelka-Munk transformation:⁹ $\alpha \sim (1-R)^2/(2R)$, where, R and α are the absolute reflectance and pseudo-absorbance,

respectively. The direct bandgaps are obtained by taking the intercept upon extrapolation of the linear regions of $(\alpha h\nu)^2$ vs $E(\text{eV})$ plot.

Solid-State Nuclear Magnetic Resonance (NMR) Spectroscopy:

Lead-207 NMR: ^{207}Pb NMR data were acquired under non-spinning conditions for samples packed in 4 mm OD ZrO_2 rotors at 11.75 and 21.14 T, on a Bruker Avance 500 and Avance II 900 NMR spectrometers, respectively. All ^{207}Pb NMR data were collected using a 4 mm double resonance H/X Bruker probe, using a Hahn-echo pulse sequence¹⁰ i.e., $(\pi/2)_x - \tau_1 - (\pi)_y - \tau_2 - \text{ACQ}$, where τ_1 and τ_2 are the inter-pulse and refocusing delays, respectively, or a modified quadrupolar-echo pulse sequence to achieve broader excitation width and minimize line distortions at higher magnetic field strengths. A recycle delay of 4 - 20 s was used for the samples. For the MHP samples, a variable offset cumulative spectra (VOCS)¹¹ approach was used with between three and five steps and a 30 kHz (for 11.75 T) or 50 kHz (for 21.14 T) transmitter stepping frequency across the spectral range to get a complete and undistorted spectrum; the sub-spectra were added using the skyline projection method. Two-dimensional ^{207}Pb - ^{207}Pb exchange spectroscopy (EXSY)¹² NMR spectra were acquired at 21.14 T by using mixing times between 50 μs and 50 ms. A total of 24-128 slices were collected in the indirect dimension using a 2 μs increment, and between 128 and 1,024 transients were acquired per slice. All ^{207}Pb NMR spectra were referenced to PbMe_4 ($\delta(^{207}\text{Pb}) = 0.00$ ppm) by setting $\delta(^{207}\text{Pb}) = -647.5$ ppm for solid MAPbCl_3 at 293 K.¹³

Caesium-133 NMR: ^{133}Cs NMR data were acquired at 11.75 T on a Bruker Avance 500 spectrometer under magic-angle spinning (MAS) conditions using a spinning frequency of 13 kHz. All samples were packed into 4 mm OD ZrO_2 and a Bloch pulse sequence was used with a 1.25 μs pulse width ($\sim 20^\circ$ tip angle), 1-16 co-added transients and 120 s recycle delay.

NMR Data Processing and Analysis: NMR spectra were processed using Topspin 3.5 Bruker software with between 25 and 500 Hz exponential apodization and plotted using OriginPro 8 software. The ^{207}Pb

NMR peak maxima ($\delta_{cs}^{(207\text{Pb})}$) are reported for the CsPbX_3 ($X = \text{Cl, Br, I}$) parent perovskite phases due to the broad lineshapes. The ^{207}Pb NMR chemical shift anisotropy for $\delta\text{-CsPbI}_3$ was simulated using the WSOLIDS software¹⁴.

Quantum Chemical Calculations: Cluster models of the octahedral lead halide, $[\text{PbX}_{6-x}\text{X}'_x]^{4-}$, were used to calculate the theoretical ^{207}Pb NMR shielding and tensor values. Average bond lengths were taken from the appropriate dimension crystal structure, where 3D geometries gave $r(\text{Pb-Cl}) = 2.843 \text{ \AA}$, $r(\text{Pb-Br}) = 2.966 \text{ \AA}$, and $r(\text{Pb-I}) = 3.146 \text{ \AA}$, and the 0D structures gave $r(\text{Pb-Cl}) = 2.513 \text{ \AA}$, and $r(\text{Pb-Br}) = 3.028 \text{ \AA}$.¹⁵⁻
¹⁸ Density functional theory, specifically the generalized gradient approximation functional PBE,¹⁹ was used within the Amsterdam Density Functional (ADF) program (Version 2016-07-01).²⁰⁻²² The zero order regular approximation²³ (ZORA) with the appropriate Slater-type all-electron triple-zeta polarized (ZORA/TZP) basis set was used to describe scalar relativistic effects and spin-orbit coupling present within the heavy-metal cluster. The calculations were performed without symmetry in order to generate ^{207}Pb NMR shielding and tensors incorporating relativistic effects. In order to compare calculated and experimental chemical shifts, the theoretical shielding constants were converted to chemical shifts using $\delta_{\text{calc}}(\text{ppm}) = -(\sigma_{\text{calc}} - 8583 \text{ ppm})$ for both the 3D and 0D materials. This relationship was determined from a linear regression between experimental chemical shifts and the calculated magnetic shielding values of the parent compounds for both 3D and 0D materials.

Table S1. ^{207}Pb and ^{133}Cs NMR parameters for 3D CsPbX_3 ($X = \text{Cl, Br, I}$) and 0D Cs_4PbX_6 ($X = \text{Cl, Br}$) parent perovskites ($B_0 = 11.75 \text{ T}$).

Samples	^{207}Pb non-spinning NMR		^{133}Cs MAS NMR	
	$^a\delta_{cs}^{(207\text{Pb})}/\text{ppm}$	fwhm/kHz	$\delta_{cs}^{(133\text{Cs})}/\text{ppm}$	fwhm/Hz
CsPbCl_3	-728 (1)	~ 5	76.9 (0.1)	155 (5)
CsPbBr_3	244 (5)	~ 18	110.3 (0.2)	238 (5)
Black $\gamma\text{-CsPbI}_3$	1265 (20)	~ 25	166.9 (0.3)	390 (10)
Yellow $\delta\text{-CsPbI}_3$	1065 (15) ^b	- ^c	247.0 (0.2)	385 (5)
Cs_4PbCl_6	-1139 (1)	~ 4.5	185.0 (0.1)	165 (5)
Cs_4PbBr_6	-385 (5)	~ 14	224.9 (0.1)	305 (5)

^aChemical shift at peak maxima, δ_{cs} ; ^b Isotropic chemical shift, δ_{iso} ; ^c Span (Ω) = 650 (30) ppm, skew (κ) = 0.7 (0.1)

Table S2. ^{207}Pb magnetic shielding parameters from octahedral $[\text{PbX}_{6-x}\text{X}'_x]^{4-}$ anionic clusters from DFT calculations. σ_{iso} = isotropic shielding constant, Ω = span, and κ = skew.

(a) 3D Materials:

Environments	σ_{iso} (ppm)	Ω (ppm)	κ
$[\text{PbCl}_6]^{4-}$	9381.77	0.0	0
$[\text{PbCl}_5\text{Br}]^{4-}$	9239.67	10.3	0.99
cis- $[\text{PbCl}_4\text{Br}_2]^{4-}$	9098.6	9.8	0.13
trans- $[\text{PbCl}_4\text{Br}_2]^{4-}$	9102.63	15.7	0.99
fac- $[\text{PbCl}_3\text{Br}_3]^{4-}$	8959.46	3.9	-0.99
mer- $[\text{PbCl}_3\text{Br}_3]^{4-}$	8962.06	24.6	0.67
cis- $[\text{PbCl}_2\text{Br}_4]^{4-}$	8824.46	14.5	-0.87
trans- $[\text{PbCl}_2\text{Br}_4]^{4-}$	8825.71	54.9	0.99
$[\text{PbClBr}_5]^{4-}$	8690.85	31.3	0.99
$[\text{PbBr}_6]^{4-}$	8560.13	0.0	0.75
$[\text{PbBr}_5\text{I}]^{4-}$	8394.72	81.4	-1.00
cis- $[\text{PbBr}_4\text{I}_2]^{4-}$	8243.18	109.9	0.91
trans- $[\text{PbBr}_4\text{I}_2]^{4-}$	8224.02	211.9	-1.00
fac- $[\text{PbBr}_3\text{I}_3]^{4-}$	8109.09	4.9	0.99
mer- $[\text{PbBr}_3\text{I}_3]^{4-}$	8091.06	253.8	0.02
cis- $[\text{PbBr}_2\text{I}_4]^{4-}$	7978.04	143.2	-0.97
trans- $[\text{PbBr}_2\text{I}_4]^{4-}$	7963	283.4	1.00
$[\text{PbBrI}_5]^{4-}$	7873.11	152.0	0.99
$[\text{PbI}_6]^{4-}$	7796.52	0.0	0.00

(b) 0D Materials:

Environments	σ_{iso} (ppm)	Ω (ppm)	κ
$[\text{PbCl}_6]^{4-}$	9210.36	0.0	-1.00
$[\text{PbCl}_5\text{Br}]^{4-}$	8556.83	460.5	0.78
cis- $[\text{PbCl}_4\text{Br}_2]^{4-}$	8738.37	392.3	0.74
trans- $[\text{PbCl}_4\text{Br}_2]^{4-}$	8944.73	527.5	1.00
fac- $[\text{PbCl}_3\text{Br}_3]^{4-}$	8569.72	644.4	-1.00
mer- $[\text{PbCl}_3\text{Br}_3]^{4-}$	8712.53	812.4	-0.22
cis- $[\text{PbCl}_2\text{Br}_4]^{4-}$	8528.2	787.6	-0.47
trans- $[\text{PbCl}_2\text{Br}_4]^{4-}$	8758.8	1559.2	-1.00
$[\text{PbClBr}_5]^{4-}$	8509.47	896.4	-1.00
$[\text{PbBr}_6]^{4-}$	8421.84	0.0	0.00

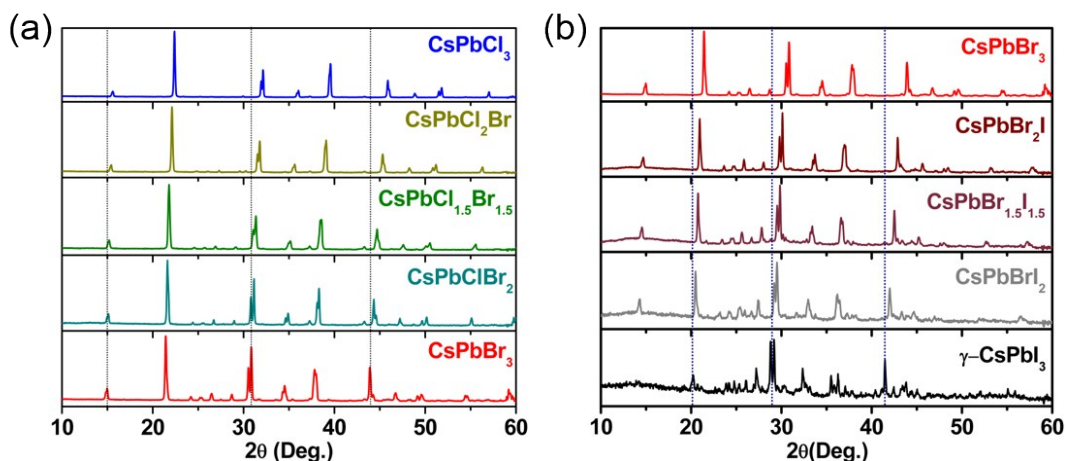


Figure S1. Room temperature powder XRD patterns for CsPbCl_xBr_{3-x} (a), and CsPbBr_xI_{3-x} (b), where $0 \leq x \leq 3$. The dotted lines are the guides to the eye.

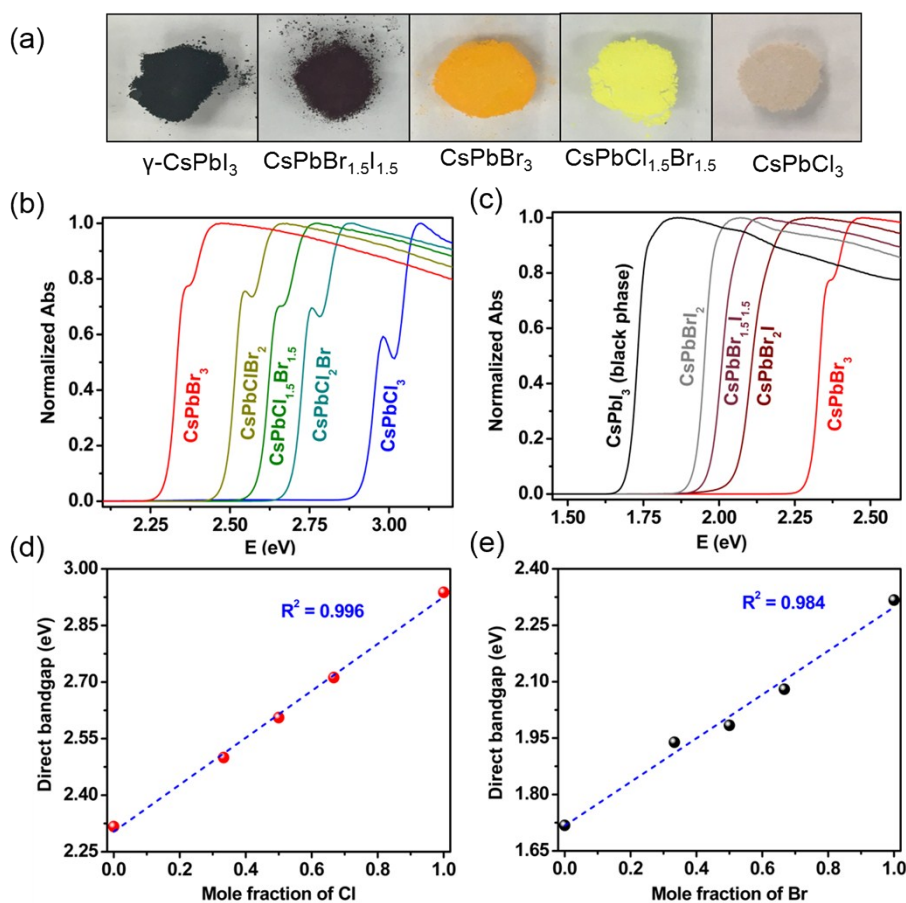


Figure S2. Photos of the 3D materials as indicated (a). Normalized absorbance spectra and direct bandgap relationship with halide composition for CsPbCl_xBr_{3-x} (b and d, respectively) and CsPbBr_xI_{3-x} (c and e, respectively), where $0 \leq x \leq 3$. The DR spectra were converted to absorbance by using the Kubelka–Munk equation and direct bandgaps are extracted from the Tauc plot (see Materials and Methods). The CsPbCl_xBr_{3-x} materials were prepared only by MCS-HG, whereas for the CsPbBr_xI_{3-x} materials, an additional thermal annealing step post-MCS was performed.

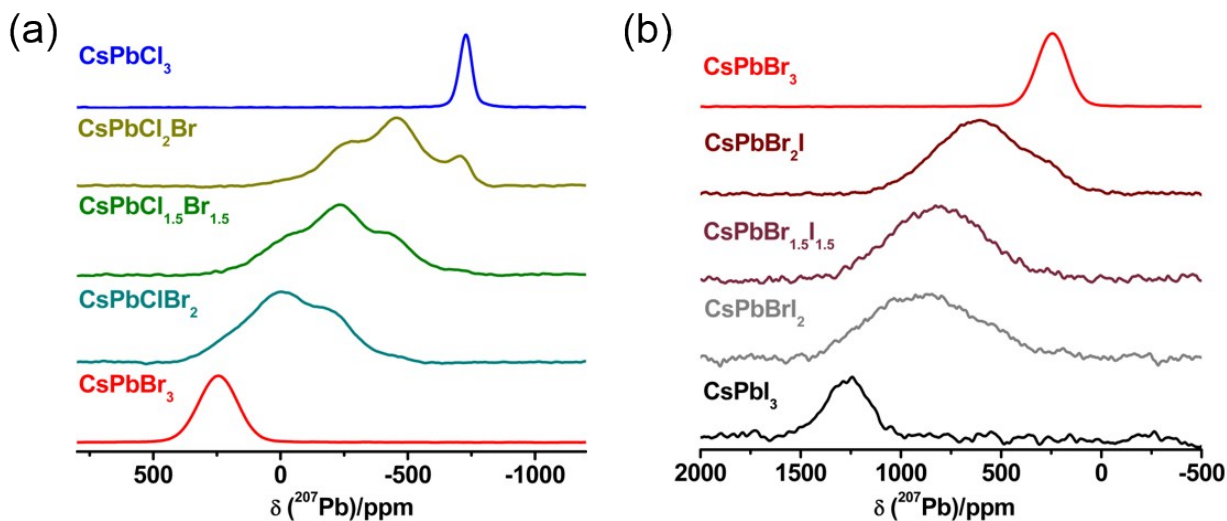


Figure S3. Room temperature ^{207}Pb NMR spectra acquired at 11.75 T under non-spinning conditions for $\text{CsPbCl}_x\text{Br}_{3-x}$ (a), and $\text{CsPbBr}_x\text{I}_{3-x}$ (b), where $0 \leq x \leq 3$. The $\text{CsPbCl}_x\text{Br}_{3-x}$ materials were prepared only by MCS-HG, whereas an additional thermal annealing step post-MCS was performed for the $\text{CsPbBr}_x\text{I}_{3-x}$ materials.

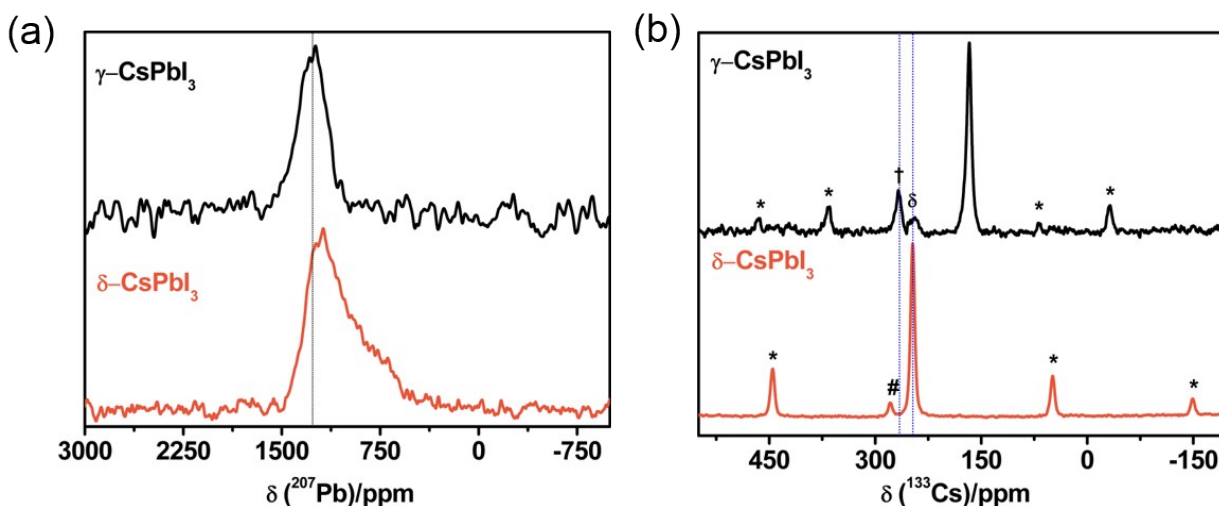


Figure S4. ^{207}Pb (a) and ^{133}Cs (b) NMR spectra for $\gamma\text{-CsPbI}_3$ (perovskite or black phase) and for $\delta\text{-CsPbI}_3$ (non-perovskite or yellow phase), acquired at 11.75 T. The ^{207}Pb NMR spectra were acquired under non-spinning sample conditions, whereas the ^{133}Cs NMR spectra were acquired under MAS conditions at a spinning frequency of 13 kHz. The non-perovskite $\delta\text{-CsPbI}_3$ phase was prepared by MCS and the corresponding perovskite phase $\gamma\text{-CsPbI}_3$ was obtained by thermal annealing at 350 °C. The dotted lines in (a) are guides to the eye showing that the ^{207}Pb NMR chemical shift for $\gamma\text{-CsPbI}_3$ is higher in frequency compared to that for $\delta\text{-CsPbI}_3$. The asterisks (*), delta (δ), crosses (\dagger), and hashtag (#) in (b) indicate spinning sidebands, $\delta\text{-CsPbI}_3$, Cs-containing impurity and residual CsI, respectively.

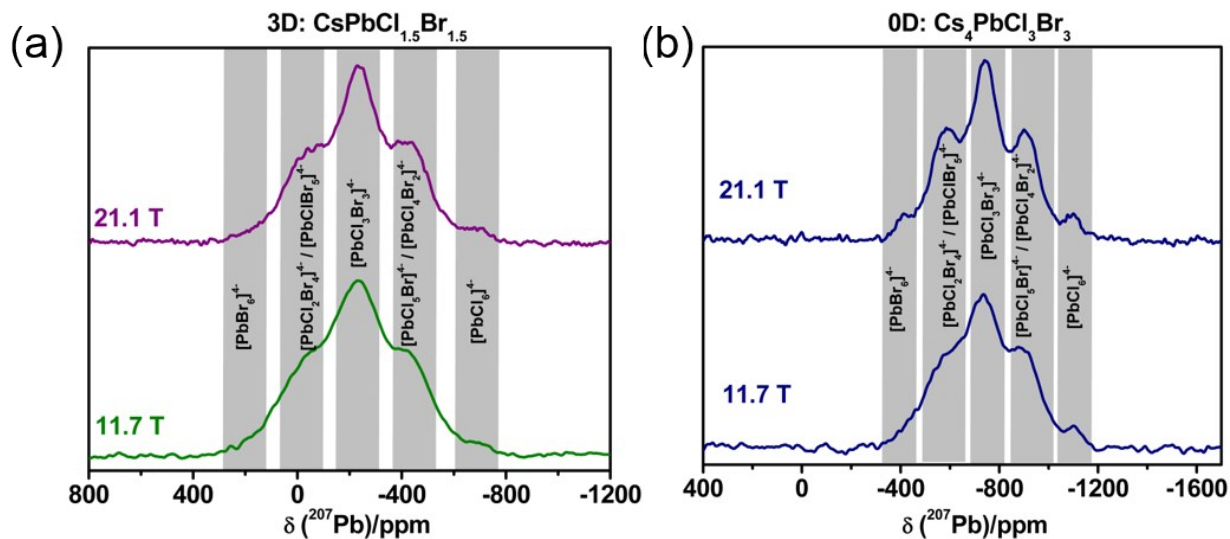


Figure S5. ^{207}Pb NMR spectra for $\text{CsPbCl}_{1.5}\text{Br}_{1.5}$ MHP (a, 3D material) and $\text{Cs}_4\text{PbCl}_3\text{Br}_3$ MHP (b, 0D material) prepared by MCS, acquired at 11.75 and 21.1 T under non-spinning sample conditions. The unique ^{207}Pb NMR chemical shifts of the corresponding DFT calculated $[\text{PbCl}_x\text{Br}_{6-x}]^{4-}$ octahedra ($x = 0$ to 6) are indicated by the highlighted regions within the spectra.

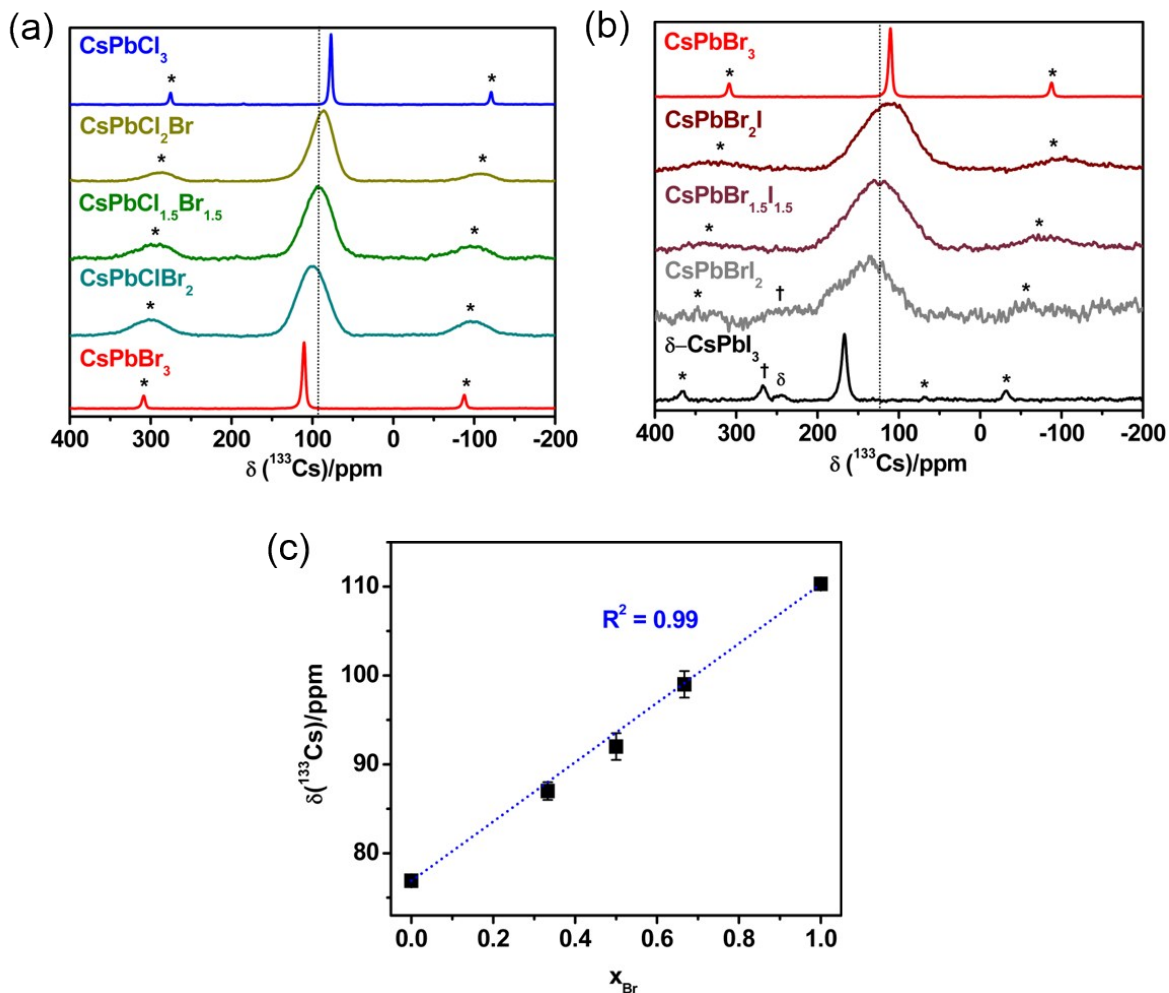


Figure S6. Room temperature ^{133}Cs NMR spectra acquired at 11.75 T with an MAS frequency of 13 kHz for the $\text{CsPbCl}_x\text{Br}_{3-x}$ (a), and $\text{CsPbBr}_x\text{I}_{3-x}$ (b) series, where $0 \leq x \leq 3$. The linear fitting of ^{133}Cs isotropic chemical shifts vs bromine mole-fraction for the $\text{CsPbCl}_x\text{Br}_{3-x}$ series is shown in (c). The $\text{CsPbCl}_x\text{Br}_{3-x}$ materials were prepared only by MCS-HG, whereas an additional thermal annealing step post-MCS was performed for the $\text{CsPbBr}_x\text{I}_{3-x}$ materials. The dotted lines in (a) and (b) are guides for the eye. The asterisks (*), dagger (†) and delta (δ) in (b) indicate spinning sidebands, Cs-containing impurity and $\delta\text{-CsPbI}_3$, respectively.

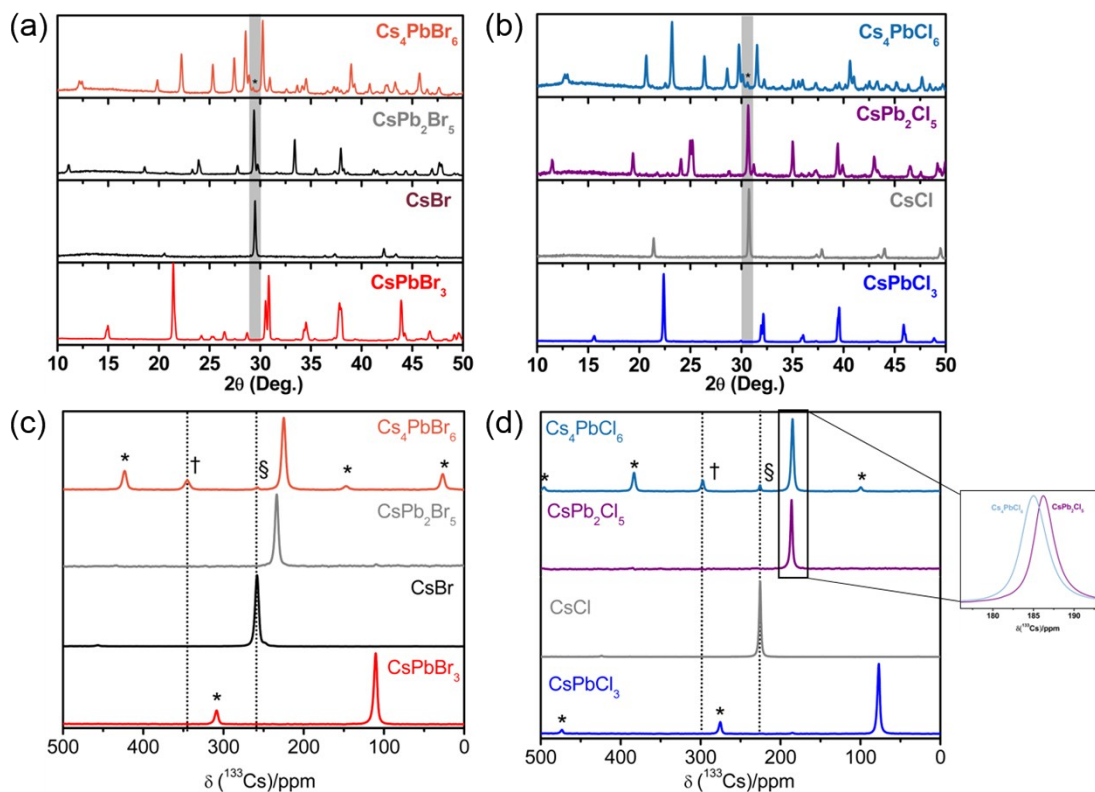


Figure S7. Room temperature powder XRD patterns (a and b) and ^{133}Cs NMR (c and d) for 0D Cs_4PbCl_6 and Cs_4PbBr_6 materials, respectively. The XRD and ^{133}Cs NMR are compared with their corresponding 2D CsPb_2X_5 , 3D CsPbX_3 and CsX ($\text{X} = \text{Cl}, \text{Br}$). All the 0D, 2D and 3D materials were prepared by MCS-HG protocol. The asterisks (*) indicate the highly intense (110) peak of CsX , a starting material. The dotted lines are guides to the eye. Insert in (d) shows the slight but distinguishable ^{133}Cs NMR chemical shift difference between 0D Cs_4PbCl_6 and 2D CsPb_2Cl_5 materials.

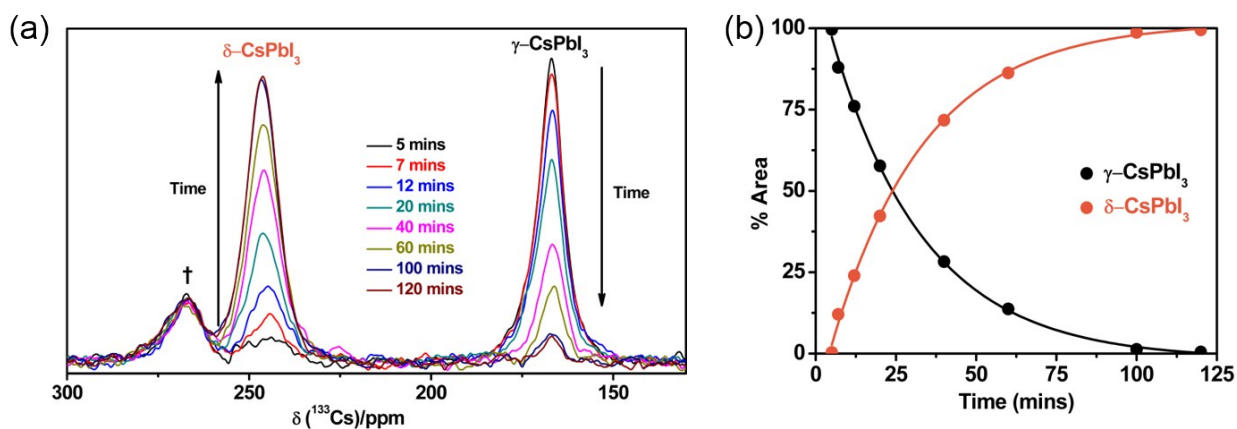


Figure S8. Room temperature ^{133}Cs NMR spectra for CsPbI_3 (a) showing the perovskite, $\gamma\text{-CsPbI}_3$, to non-perovskite, $\delta\text{-CsPbI}_3$, phase conversion over time. The freshly prepared $\gamma\text{-CsPbI}_3$ sample was packed in a 4 mm OD ZrO_2 rotor and the spectra were acquired at 11.75 T under magic-angle spinning at 13 kHz. Area (%) of ^{133}Cs NMR spectra of $\gamma\text{-}$ and $\delta\text{-CsPbI}_3$ as a function of time (b). The fitting line suggests a first-order kinetics phase conversion mechanism with a half-life ($t_{1/2}$) of 29 ± 2 mins. The dagger (\dagger) in (a) indicates Cs-containing impurity present within the sample.

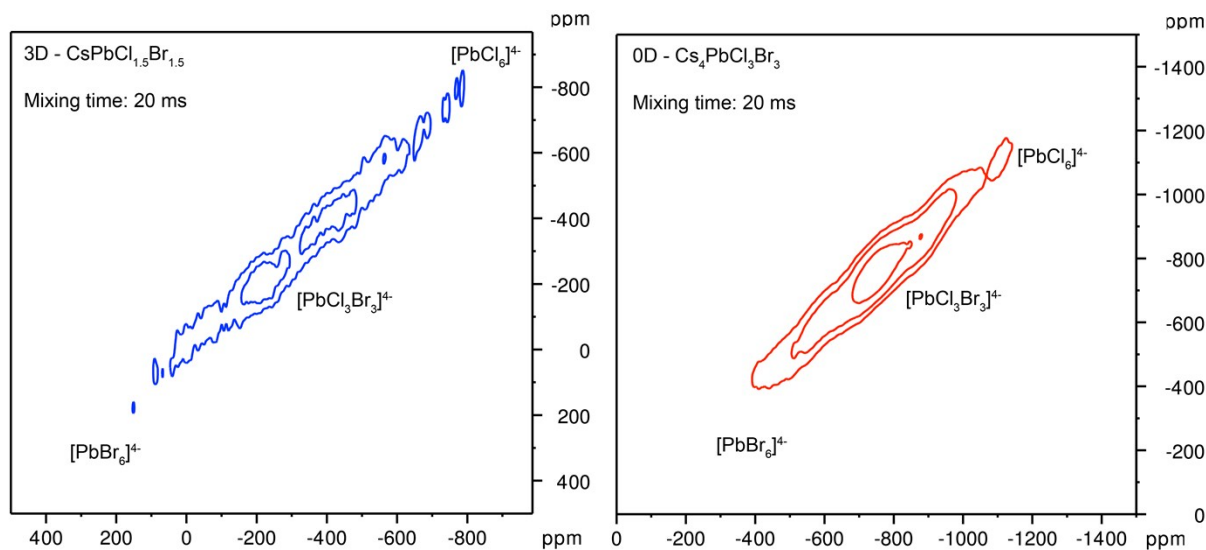


Figure S9. Room temperature non-spinning $^{207}\text{Pb}\text{-}^{207}\text{Pb}$ EXSY NMR spectra for 3D $\text{CsPbCl}_{1.5}\text{Br}_{1.5}$ (left, blue) and 0D $\text{Cs}_4\text{PbCl}_3\text{Br}_3$ (right, red) MHP materials acquired at 21.14 T with a mixing time of 20 ms.

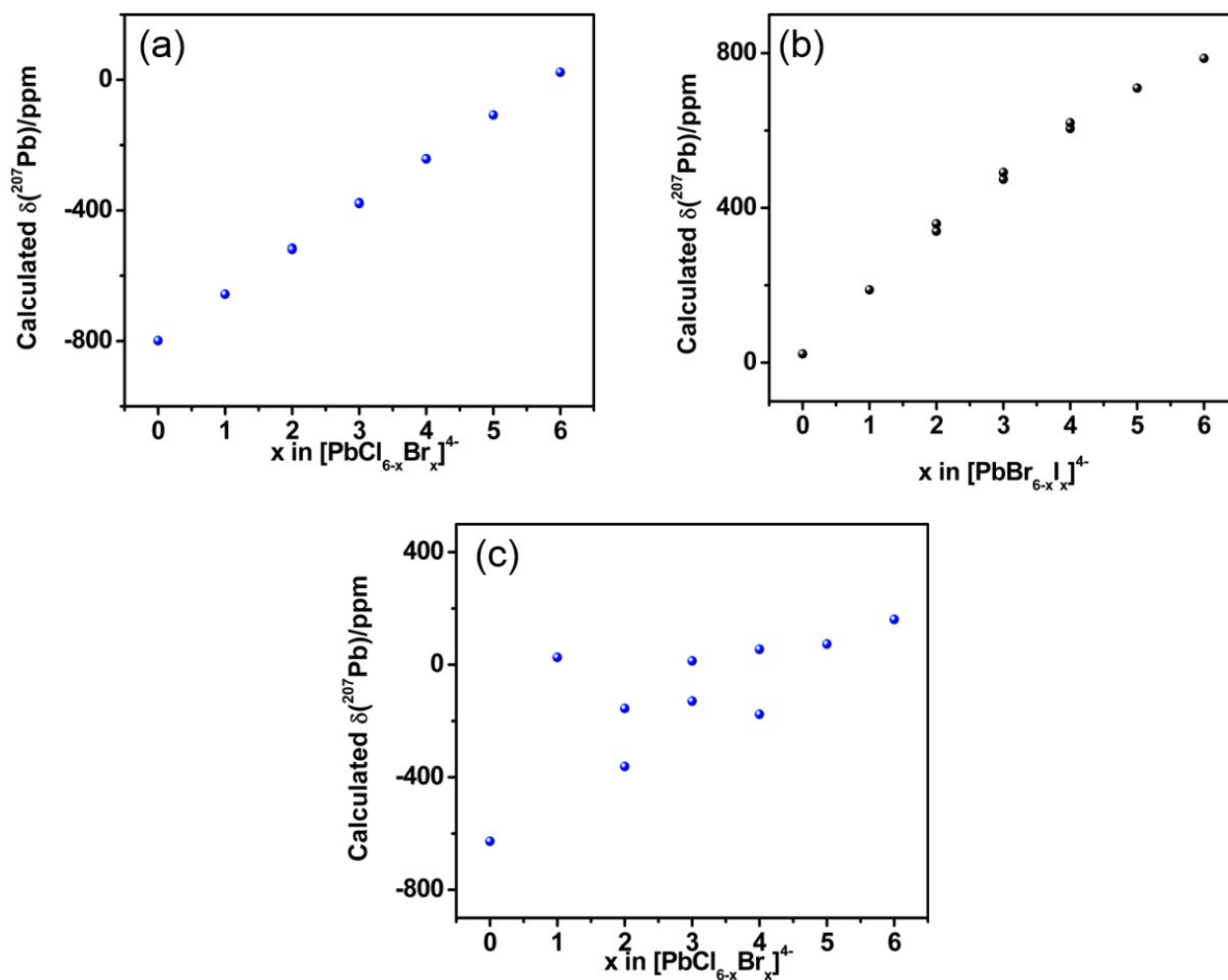


Figure S10. Calculated ^{207}Pb NMR isotropic chemical shift with Br substitution in $[\text{PbCl}_{6-x}\text{Br}_x]^{4-}$ polyhedral (a, 3D materials), I substitution in $[\text{PbBr}_{6-x}\text{I}_x]^{4-}$ polyhedral (b, 3D materials), and Br substitution in $[\text{PbCl}_{6-x}\text{Br}_x]^{4-}$ polyhedral (c, 0D materials), where, $x = 0$ to 6.

REFERENCES

- 1 J. Breternitz, S. Levchenko, H. Hempel, G. Gurieva, A. Franz, A. Hoser and S. Schorr, *arXiv*, 2018, (<https://arxiv.org/ftp/arxiv/papers/1810/1810.1133>).
- 2 S. Yun, A. Kirakosyan, S. Yoon and J. Choi, *ACS Sustain. Chem. Eng.*, 2018, **6**, 3733–3738.
- 3 M. Wilke and N. Casati, *Chem. - A Eur. J.*, 2018, **24**, 17701–17711.
- 4 O. Y. Posudievsky, N. V. Konoshchuk, A. G. Shkavro, V. L. Karbivskiy, V. G. Koshechko and V. D. Pokhodenko, *ACS Appl. Nano Mater.*, 2018, **1**, 4145–4155.
- 5 D. J. Kubicki, D. Prochowicz, A. Hofstetter, S. M. Zakeeruddin, M. Grätzel and L. Emsley, *J. Am. Chem. Soc.*, 2018, **140**, 7232–7238.
- 6 D. Prochowicz, P. Yadav, M. Saliba, M. Sasaki, S. M. Zakeeruddin, J. Lewinski and M. Gratzel, *Sustain. Energy Fuels*, 2017, **1**, 689–693.
- 7 A. D. Jodlowski, A. Yépez, R. Luque, L. Camacho and de G. Miguel, *Angew. Chemie Int. Ed.*, 2016, **55**, 14972–14977.
- 8 Z. Zhu, Q. Yang, L. Gao, L. Zhang, A. Shi, C. Sun, Q. Wang and H. Zhang, *J. Phys. Chem. Lett.*, 2017, **8**, 1610–1614.
- 9 P. Kubelka and F. Munk, *Z. Tech. Phys. (Leipzig)*, 1931, **12**, 593–601.
- 10 E. L. Hahn, *Phys. Rev.*, 1950, **80**, 580–594.
- 11 D. Massiot, I. Farnan, N. Gautier, D. Trumeau, A. Trokner and J. Pierre, *Solid State Nucl. Magn. Reson.*, 1995, **4**, 241–248.
- 12 J. Jeener, B. H. Meier, P. Bachmann and R. R. Ernst, *J. Chem. Phys.*, 1979, **71**, 4546–4553.
- 13 G. M. Bernard, A. Goyal, M. Miskolzie, R. McKay, Q. Wu, R. E. Wasylshen and V. K. Michaelis, *J. Magn. Reson.*, 2017, **283**, 14–21.
- 14 K. Eichele, *WSOLIDS NMR Simulation Package, 1.21.3; Universität Tübingen: Tübingen, Germany*, 2013.
- 15 M. Natarajan and B. Prakash, *Phys. Status Solidi A Appl. Res.*, 1971, **4**, K167–K172.
- 16 C. C. Stoumpos, C. D. Malliakas, J. A. Peters, Z. Liu, M. Sebastian, J. Im, T. C. Chasapis, A. C. Wibowo, D. Y. Chung, A. J. Freeman, B. W. Wessels and M. G. Kanatzidis, *Cryst. Growth Des.*, 2013, **13**, 2722–2727.
- 17 R. J. Sutton, M. R. Filip, A. A. Haghighirad, N. Sakai, B. Wenger, F. Giustino and H. J. Snaith, *ACS Energy Lett.*, 2018, **3**, 1787–1794.
- 18 M. De Bastiani, I. Dursun, Y. Zhang, B. A. Alshankiti, X. H. Miao, J. Yin, E. Yengel, E. Alarousu, B. Turedi, J. M. Almutlaq, M. I. Saidaminov, S. Mitra, I. Gereige, A. Alsaggaf, Y. Zhu, Y. Han, I. S. Roqan, J. L. Bredas, O. F. Mohammed and O. M. Bakr, *Chem. Mater.*, 2017, **29**, 7108–7113.
- 19 J. P. Perdew, K. Burke and M. Ernzerhof, *Phys. Rev. Lett.*, 1996, **77**, 3865–3868.
- 20 G. te Velde, F. M. Bickelhaupt, E. J. Baerends, C. Fonseca Guerra, S. J. A. van Gisbergen, J. G. Snijders and T. Ziegler, *J. Comput. Chem.*, 2001, **22**, 931–967.
- 21 C. F. Guerra, J. G. Snijders, G. te Velde and E. J. Baerends, *Theor. Chem. Acc.*, 1998, **99**, 391–403.
- 22 E. J. Baerends, T. Ziegler, A. J. Atkins, J. Autschbach, D. Bashford, O. Baseggio, A. Bérces, F. M. Bickelhaupt, C. Bo, P. M. Boerritger, L. Cavallo, C. Daul, D. P. Chong, D. V. Chulhai, L. Deng, R. M. Dickson, J. M. Dieterich, D. E. Ellis, M. van Faassen, A. Ghysels, A. Giammona, S. J. A. van Gisbergen, A. Goez, A. W. Götz, S. Gusarov, F. E. Harris, P. van den Hoek, Z. Hu, C. R. Jacob, H. Jacobsen, L. Jensen, L. Joubert, J. W. Kaminski, G. van Kessel, C. König, F. Kootstra, A. Kovalenko, M. Krykunov, E. van Lenthe, D. A. McCormack, A. Michalak, M. Mitoraj, S. M. Morton, J. Neugebauer, V. P. Nicu, L. Noodleman, V. P. Osinga, S. Patchkovskii, M. Pavanello, C. A. Peeples, P. H. T. Philipsen, D. Post, C. C. Pye, H. Ramanantoanina, P. Ramos, W. Ravenek, J. I. Rodríguez, P. Ros, R. Rüger, P. R. T. Schipper, D. Schlüns, H. van Schoot, G. Schreckenbach, J. S. Seldenthuis, M. Seth, J. G. Snijders, M. Solà, S. M., M. Swart, D. Swerhone, G. te Velde, V. Tognetti, P. Vernooijs, L. Versluis, L. Visscher, O. Visser, F. Wang, T. A. Wesolowski, E. M. van Wezenbeek, G. Wiesenecker, S. K. Wolff, T. K. Woo and A. L. Yakovlev, *ADF2018, SCM, Theor. Chem. Vrije Univ. Amsterdam, Netherlands*, <http://www.scm.com>.
- 23 P. Philipsen, E. van Lenthe, J. Snijders and E. Baerends, *Phys. Rev. B*, 1997, **56**, 13556–13562.